Ecological Engineering 118 (2018) 179–190

Contents lists available at ScienceDirect

Ecological Engineering

journal homepage: www.elsevier.com/locate/ecoleng

Assessment of the water cycle impact by the Budyko curve on watershed hydrology using SWAT and CO_2 concentrations derived from Terra MODIS GPP

Chung Gil Jung, Seong Joon Kim*

Konkuk University, Dept. of Civil and Environmental engineering, 1 Hwayang-dong, Gwangjin-gu, Seoul 143-701, South Korea

ARTICLE INFO

Keywords:
Carbon dioxide
CO_2 flux
Climate change
SWAT
MODIS GPP
Water cycle
Budyko curve

ABSTRACT

Greenhouse gas and aerosol emissions from human activities continue to alter the climate and are likely to have significant impacts on watershed hydrological cycles and stream water quality. We applied the Soil and Water Assessment Tool (SWAT) to evaluate how CO_2 impacts the hydrology of a watershed. The goal of this study is to evaluate how potential CO_2 changes would impact the hydrologic components in the forest-dominant Seolmacheon watershed (8.48 km^2) in South Korea. Using an image from the Moderate Resolution Imaging Spectroradiometer (MODIS) onboard Terra, the CO_2 flux was estimated as the sum of the Gross Primary Productivity (GPP) and Ecosystem Respiration (R_{ec}) following the method of Lloyd and Taylor (1994). To assess the water cycle impact, the SWAT results for certain hydrological components, such as total runoff (TQ), surface runoff (SQ), lateral runoff (LQ), soil water content (SW) and evapotranspiration (ET), were analysed to generate Budyko curves. In the field of watershed management, SWAT modelling using CO_2 concentrations as an additional parameter provides a better understanding of the role of ET and soil moisture in ongoing and future climate changes.

1. Introduction

Fossil fuel consumption has caused an increase in the anthropogenic emissions of carbon dioxide (CO_2) and other greenhouse gases for a long time. Climate change caused by the emissions of greenhouse gases and aerosols from human activities continue to alter the climate and is likely to have significant impacts on watershed hydrological cycles and stream water quality. Recently, many studies have investigated the impact of the effects of climate change on water resource changes. Using the Soil and Water Assessment Tool (SWAT) model, Zhang et al. (2007) estimated an average 10% increase in runoff by applying the A2 and B2 climate change scenario results. Ahn et al. (2016) assessed the impacts of future climate change on the water balance by considering the agricultural water supply capacity. Moreover, Ahn et al. (2016) estimated an average 6.9% increase in runoff based on the RCP4.5 scenario.

Prior to the Industrial Revolution, global CO_2 concentration in the air ranged from 260 to 290 ppm (ppm) (Kimball and Idso, 1983), whereas the current CO_2 content is approaching 400 ppm, thus representing a 45% increase, which is primarily because of the burning of fossil fuels. Predictions by the Intergovernmental Panel on Climate Change (IPCC) indicate that CO_2 concentration in the atmosphere will approach 700 ppm at the end of this century and possibly as early as 2025. In South Korea, the Korea Meteorological Administration (KMA) has been operating a climate change watch centre to monitor the global atmosphere at 5 stations. These stations have monitored 37 atmospheric components, including greenhouse gases, aerosols, and atmospheric radiation. In particular, the CO_2 concentration consistently increased from 370.7 ppm to 407.0 ppm from 1999 to 2015 at the Anmyeondo station (Korea Meteorological administration, 2015).

Atmospheric CO_2 concentrations directly cause a physiological reaction in plant growth by impacting the CO_2 absorption rate and stomatal resistance (Morison and Gifford, 1984). Stomatal resistance changes to regulate the respiratory rate and the absorption rate of CO_2 for photosynthesis. Increases in atmospheric CO_2 increase the internal CO_2 absorption rate in leaves. As a result, the plant reacts by increasing stomatal resistance, which reduces the CO_2 absorption rate. Eventually, the increased stomatal resistance reduces the transpiration from the leaves to the atmosphere (Morison, 1987), which reduces the water-use requirements and increases the water-use efficiency of plants.

Many studies based on observations and modelling have implied that increased CO_2 concentrations and climate change have significant

* Corresponding author at: 1 Hwayang-dong, Gwangjin-gu, Seoul 143-701, South Korea.
E-mail address: kimsj@konkuk.ac.kr (S.J. Kim).

https://doi.org/10.1016/j.ecoleng.2018.05.005
Received 30 January 2018; Received in revised form 10 April 2018; Accepted 4 May 2018
Available online 12 May 2018
0925-8574/

impacts on hydrological systems. However, few approaches are available that can consistently quantify atmospheric CO_2 concentration in watersheds. To overcome this problem, the potential impacts of CO_2 concentrations can be quantified for a specific watershed using hydrological models. For example, SWAT (Arnold et al., 2008; Neitsch et al., 2005) has been widely used to evaluate hydrological processes and ecological water environment in a watershed. More recently, Wu et al. (2012) modified SWAT (version 2005) to better represent more mechanistic vegetation responses to elevated CO_2 concentrations, such as reduced stomatal conductance and increased leaf area.

The overall goal of this study was to evaluate how potential CO_2 changes impact the hydrologic components in the forest-dominant Seolma-cheon watershed (8.48 km^2) in South Korea. The specific objectives of the study were as follows: (1) to estimate the atmospheric CO_2 concentration by using Terra Moderate Resolution Imaging Spectroradiometer (MODIS) Gross Primary Productivity (GPP) data and the Lloyd and Taylor method; (2) to modify the original SWAT module to allow for application of the estimated atmospheric CO_2 concentrations; (3) to analyse the SWAT results and determine the impact on hydrologic components; and (4) to assess water cycle changes using the Budyko curve (Fig. 1).

2. Materials and method

In this study, satellite data and various observed point data were used (Fig. 1). We used weather data from the Korea Meteorological Administration (KMA). This study used evapotranspiration (ET) and soil moisture (SM) data measured by the Hydrological Survey Center (HSC). Moreover, observed CO_2 data were provided by HSC at the flux tower. Nevertheless, the model simulation period of each data is different in this study as the result of data availability.

2.1. Study watershed description

In this study, the Seolma-cheon watershed in the Han River basin was selected as the study watershed, and multiple calibrations of the hydrologic components, such as streamflow, evapotranspiration, and soil moisture, were performed. The study watershed (8.48 km^2) is located within the latitude range of 37° 55′ 25″ N to 37° 56′ 50″ N and longitude range of 126° 55′ 30″ E to 126° 57′ 30″ E. As shown in Fig. 2, four rainfall stations and one weather station were selected to generate the weather input data. To calibrate the hydrologic components, a streamflow station at the watershed outlet and evapotranspiration (ET) station and soil moisture (SM) station at the flux tower were selected. Weather data from 2003 to 2012 were analysed; the average annual precipitation was 1210 mm, and the annual mean temperature was 10.3 °C. The land use type is dominated by forest at 88.1% and upland crop at 2.2%. Moreover, the soil type is dominated by sandy loam at 76.4%.

2.2. MODIS GPP

GPP is the annual photosynthetic carbon uptake of all leaves over an area of land, and GPP and its partitioning between plant autotrophic respiration and net primary productivity (NPP) are key measures of the linkages among solar energy, atmospheric CO_2, and the terrestrial biosphere. To observe the physical variables of the land, ocean, and atmosphere over a wide spectral range (0.4–14.4 lm) and at a high spatial resolution (500 m), MODIS is used as a multipurpose satellite instrument (Justice et al., 1998). MODIS GPP/NPP is the main part of

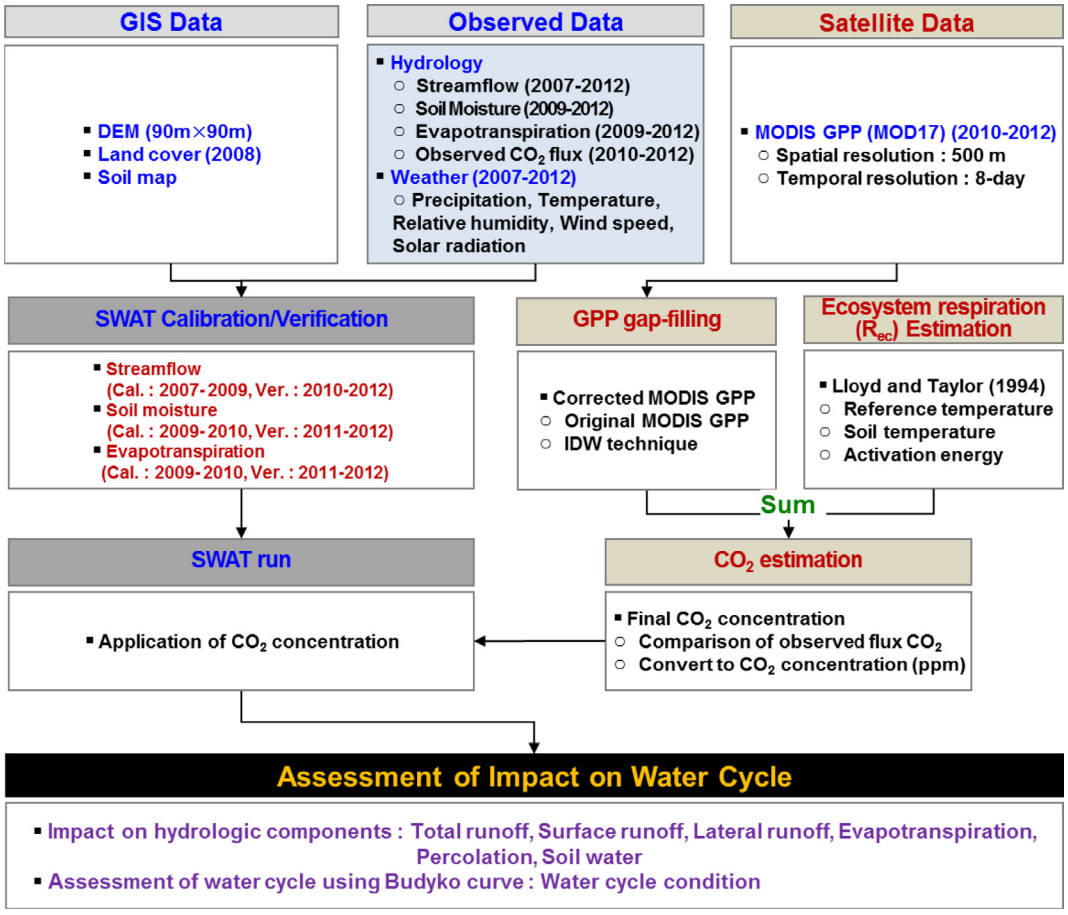

Fig. 1. Flow chart of the study.

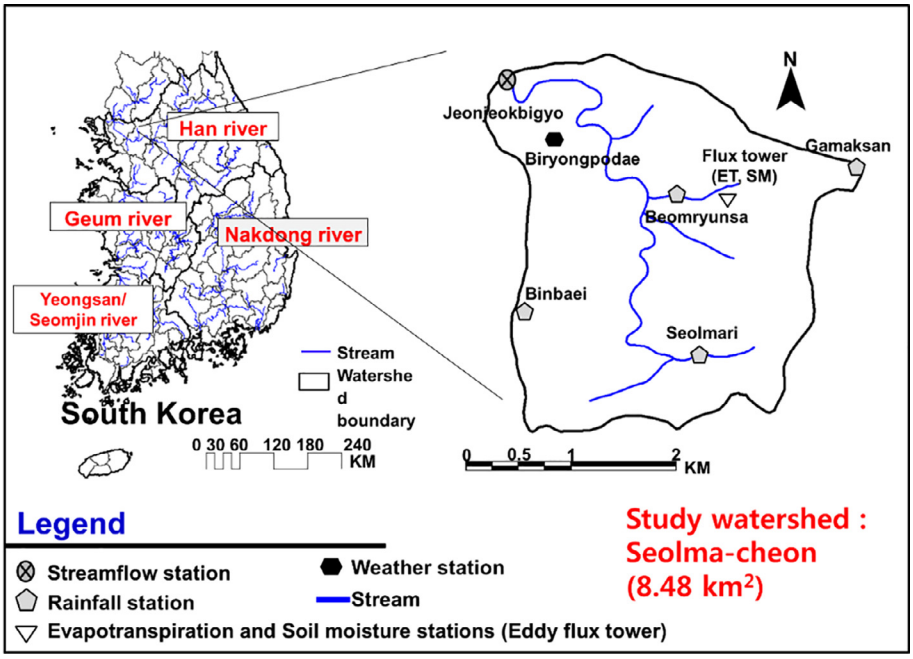

Fig. 2. Location of the study watershed and hydrological component gauging stations for hydrological modelling.

the MODIS product MOD17 (Heinsch et al., 2003; Justice et al., 2002) and has provided the first continuous satellite-based vegetation productivity data. The MOD17A2 product is available and supported by the Numerical Terradynamic Simulation Group (NTSG) (ftp://ftp.ntsg.umt.edu/pub/). The data have been widely used and validated for global and regional studies in various fields (Nemani et al., 2003; Turner et al., 2003; Sims et al., 2006; Zhao and Running, 2010). The MODIS product used here is based on Monteith's theory, which defines NPP as linearly related to the amount of absorbed PAR (Monteith, 1972; Monteith and Moss, 1977). Additionally, detailed information on the MODIS GPP/NPP algorithm can be found in the MODIS GPP/NPP manual (Thornton et al., 2002, et al., 2000; Zhao et al., 2011).

2.2.1. Development of CO_2 flux

2.2.1.1. Relationship between GPP and CO_2. GPP represents the gross primary production of the forest, and ecosystem respiration (R_{ec}) is the sum of the above-ground biomass respiration and CO_2 flux from the soil surface (including root respiration). GPP estimates are based on the measured net flux of carbon from the vegetation/soil to the atmosphere (called net ecosystem exchange, NEE) and an estimation of the terrestrial R_{ec} according to

$$NEE = GPP - R_{ec} \quad (1)$$

where NEE denotes the quantity of CO_2 flux in the ecosystem (Jung et al., 2014). In the present study, one day is defined not as a calendar day but the period from the evening when the short-wave radiation becomes zero to the next evening. This definition more accurately conveys how atmospheric CO_2 is stored in the canopy at night (or in the evening) and is released back to the atmosphere after sunrise, when radiation and boundary layer growth are increased. In the absence of horizontal advection, the daily integrated CO_2 flux will be equal to the daily NEE because the 24-h storage term must be zero for mass conservation (Saigusa et al., 2002).

2.2.1.2. Lloyd and Taylor method for estimation of R_{ec}. Reichstein et al. (2005) proposed a method of estimating R_{ec} by determining the nighttime temperature sensitivities of R_{ec} and extrapolating these estimates to the daylight period following Lloyd and Taylor (1994):

$$R_{ec} = R_{ref} \cdot e^{AE_0\left(\frac{1}{T_{ref}-T_0}-\frac{1}{T_{soil}-T_0}\right)} \quad (2)$$

where T_0 is a regression parameter with a constant of -46.02 °C, T_{ref} is the reference temperature and equal to 10 °C, and T_{Soil} is the soil temperature. R_{ref} is the temperature-dependent contribution of respiration, and AE_0 is the free parameter of activation energy and used to determine the temperature dependency (Reichstein et al., 2005).

2.3. SWAT model

SWAT is a physically based semi-distributed model for long-term and continuous predictions of hydrology and water quality under varying conditions, such as soil properties, topography, weather, vegetation, land use, and watershed management (Arnold et al., 2008). A detailed description of the SWAT model was provided by Neitsch et al. (2001). The ET as simulated by SWAT is based on the canopy resistance equation related to CO_2 concentration. The stomatal resistance is directly proportional to the canopy resistance. This ET method has an inverse relationship with γ_c.

$$\gamma_c = \gamma_l \cdot \left[(0.5 \cdot LAI) \cdot (1.4 - 0.4 \cdot \frac{CO_2}{330}) \right]^{-1} \quad (3)$$

where γ_c is the canopy resistance (s/m), γ_l is the minimum effective stomatal resistance of a single leaf (s/m), LAI is the leaf area index of the canopy, and CO_2 is the concentration of carbon dioxide in the atmosphere (ppmv) (Reichstein et al., 2005).

2.4. Budyko curve

The Budyko hypothesis (Budyko, 1974) states that the annual water balance can be expressed as a function of the available water and energy. Choudhury (1999) introduced an empirical equation of the annual evaporation basis on the earlier work by Pike (1964). Based on a dimensional analysis and mathematical reasoning, Yang et al. (2008) analytically derived the water-energy balance equation at the mean annual time scale, and the equation is expressed as follows:

$$E = \frac{PE_0}{(P^n + E_0^n)^{1/n}} \quad (4)$$

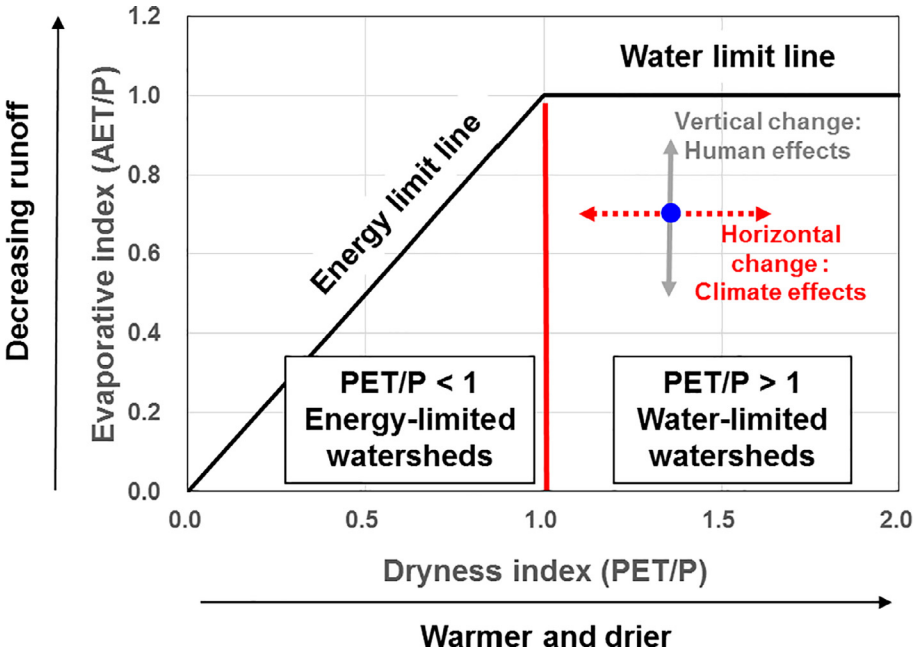

Fig. 3. Budyko curve and diagram showing the direct human and climate contributions to the mean annual streamflow change.

where E is the mean annual actual evaporation, P is the mean annual precipitation, E_0 is the mean annual potential evaporation and n represents the free parameter, which is mainly related to the properties of soil, topography and vegetation (Yang et al., 2008, 2009). Eq. (4) was referred to as the Choudhury–Yang equation by Roderick and Farquhar (2011). In this study, the value of n was related to the atmospheric CO_2 concentration. The SWAT evapotranspiration and runoff results are compared by applying the estimated CO_2 concentration from 2004 to 2012.

Based on worldwide data for a large number of watersheds, Budyko demonstrated that the ratio of the mean annual evaporation to the mean annual precipitation (E/P, evaporation ratio) is primarily controlled by the ratio of the mean annual potential evaporation to the mean annual precipitation (E_0/P, climatic dryness index) as shown in Fig. 3. For watersheds with E_0/P values less than 1, the energy supply is the limiting factor for evaporation, whereas for watersheds with E_0/P values larger than 1, the water supply is the limiting factor. Watersheds in different climatic regions fall at different points along the Budyko curve depending on the values of E_0/P. Observations from real watersheds are scattered around the Budyko curve because other factors in addition to the dryness index can also affect the partitioning of the mean annual precipitation, such as the soil water storage (Milly, 1994), vegetation (Zhang et al., 2001; Donohue et al., 2007, 2010; Yang et al., 2009), infiltration capacity, slope (Yang et al., 2007), rainfall seasonality and characteristics (Gerrits et al., 2009; Jothityangkoon and Sivapalan, 2009).

3. Results and discussion

3.1. Gap filling of MODIS GPP for cloud correction

The MODIS GPP data have missing values because of clouds and atmospheric conditions. Therefore, the MODIS GPP was regenerated by gap filling, which was performed each day with bias correction using the following equation recommended by the interpolation technique. In general, the gap-filling method was applied using the Inverse Distance Weighted (IDW) interpolation approach (Alexandridis et al., 2013), which is based on interpolating the missing values at the gaps using the existing values.

In this study, the gap-filling technique includes the following process: (a) original MODIS GPP data and QC (Quality Control) flags that constitute numerical data are collected; (b) the QC flag data can explain whether the pixels are polluted by clouds, and QC flag data provide the polluted numbers such as 0, 1, 32, 33, 64, 65, 96, and 97 per grid; (c) to correct missing values, MODIS GPP data corresponding to the polluted number such as 0, 1, 32, 33, 64, 65, 96, 97 are removed; (d) the remaining GPP data except for the polluted number convert point data; (e) (d) is interpolated by IDW. Finally, (e) is gap-filled data. Before cloud removal, the results show that the original GPP presented a trend with repeated rapid increases and sudden decreases from June to August 2010–2012 (Fig. 4(a)). In contrast, the GPP corrected by gap filling shows a gradual decline for the same season.

Generally, the GPP value range from 0 to 80 g·C/m^2 at 8-day intervals in the forest. In addition, the GPP value remained at zero during winter, increased gradually after March and reached its peak in late July to early August. After its peak, the GPP value declined in autumn and reached zero again in winter (Wang et al., 2010). In this study, after gap filling, the GPP value increased rapidly in late March to early May and then continued increasing until its peak was reached in late June to early July, and it then declined rapidly after late July to early October.

After the gap-filling process, the monthly GPP changed by + 17.4, +27.1, +13.6, +22.2, +2.2, +3.1, +19.6, +3.5, −1.2, −15.9, −17.9, and −24.5% compared to the original MODIS GPP values, respectively. In particular, the original GPPs in April and July were underestimated by 28.3 and 40.7 g·C/m^2/month. The biases show that the original GPP rapidly decreased during the rainy season in summer because of the monsoon climate in South Korea. As a result, a gap-filling process would reduce the error by an average of 19.0% in summer.

From these results, the seasonal GPP changes illustrate the timing of leaf emergence, peak leaf area and production, and leaf senescence and dormancy. In spring, as the temperature warmed and the days became longer, plants emerged, photosynthesis began, and GPP increased gradually. In fall, the leaves start to die naturally and the photosynthetic absorption of CO_2 gradually decreases because of leaf senescence before a significant decrease in leaf area occurs. As a result, GPP decreased gently (Wang et al., 2010).

3.2. Estimation of R_{ec}

In this study, the Rec value was estimated based on the flux

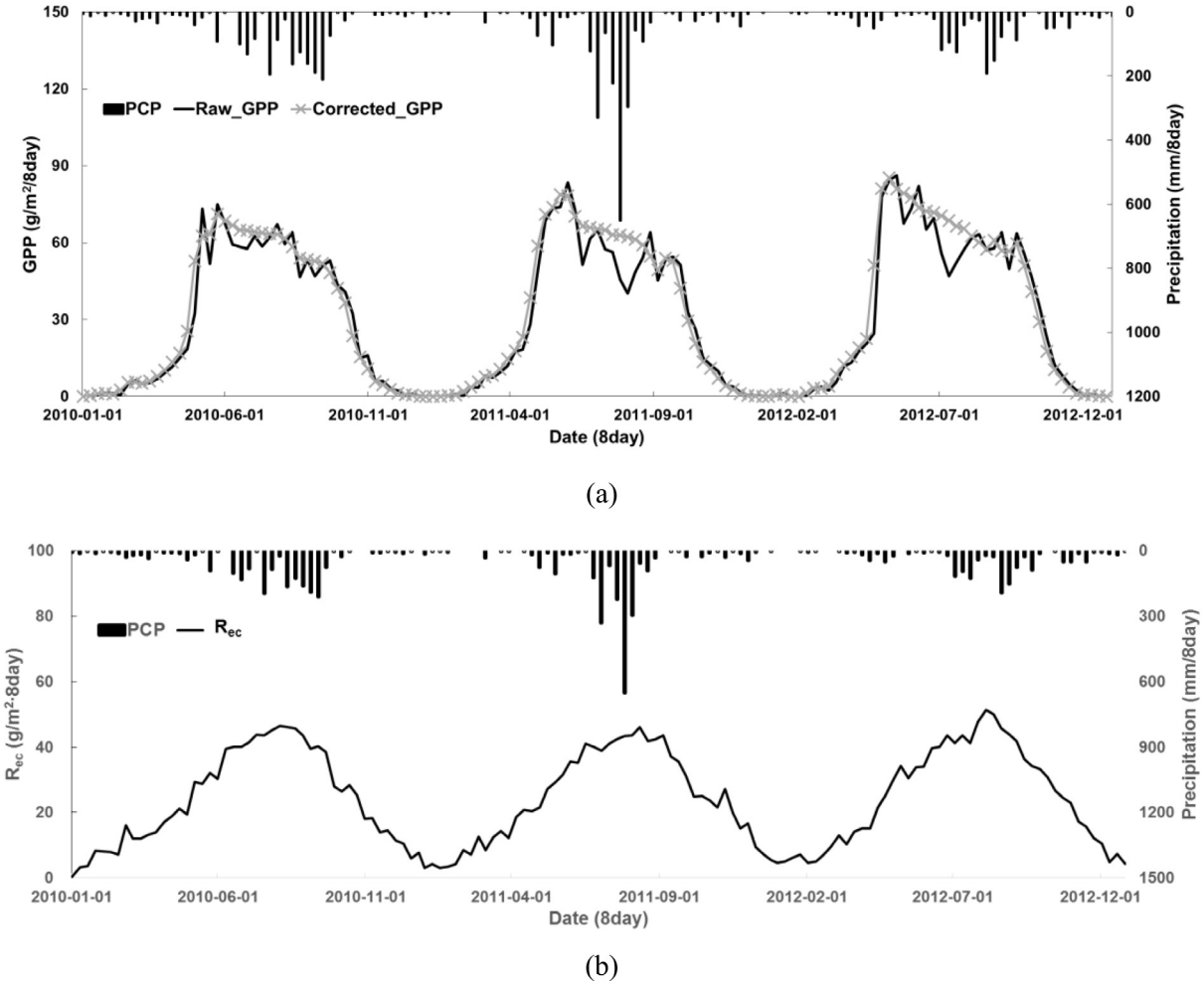

Fig. 4. Comparison of the graphs: (a) GPP values before and after gap filling, (b) the estimated Rec using the Lloyd and Taylor (1994) equation.

measurement data recorded in all experimental basins (experimental catchments). To determine the R_{ec} value, the R_{ref}, standard R_{ec} and activation energy AE_0 must be calculated empirically. A previous study conducted an experiment in southeastern China (26° 44′ 52 ″N, 115° 03′ 47 ″E, altitude 102 m) and assessed the standard R_{ec} and activation energy as empirical constants with values of 309 K and 0.77 mg/m·s, respectively (Wen et al., 2006). Because of the potentially dissimilar climate and geographical conditions in South Korea and China, a separate set of empirical constants should be calculated for watershed environments in South Korea.

Empirical constant estimations were performed using methods proposed by Van Gorsel et al. (2007) and Hong et al. (2009). The maximum CO_2 flux was measured near sunset between 6 PM and 8 PM and set as the R_{ec} value of the day. This method, which was verified in previous studies, is widely used for estimating the night-time turbulence flux. Using the Lloyd and Taylor method, the regression equation was derived to estimate the South Korean empirical constants of respiration R_{ref} and activation energy AE_0. As a result, R_{ref} was calculated at 0.054 mg/m·s and AE_0 was calculated at 204.8 K. The results of the estimated R_{ec} derived from the estimated R_{ref} and E_0 are shown in Fig. 4(b). In general, R_{ec} ranged from 1 g/m^2·day to 15 g/m^2·day (Ni et al., 2013). This result indicates that R_{ec} has a suitable value based on the general R_{ec} ranges.

In this study, R_{ec} ranged from an average of 0.26 to 52.8 g/m^2·8-day for 3 years. As a result, R_{ec} shows an obvious seasonal pattern at the mixed forest site from 2010 to 2012. The maximum 8-day mean R_{ec} usually occurred at the mid-growing period and corresponded to the tendency of maximum soil temperature and GPP values. In contrast, during the non-growing season including spring or winter dormant periods, the R_{ec} was small and coincident with the tendency towards minimum GPP values.

3.3. Estimation of CO_2

Using Eq. (1), the CO_2 flux was calculated with the corrected MODIS GPP and the estimated R_{ec}. Fig. 5 shows the estimated CO_2 flux from the MODIS GPP and the R_{ec} estimated using the Lloyd and Taylor method. Because the spikes in the observed CO_2 flux data from the flux tower may affect the quality of the gap-filled data, they were removed using an outlier detection technique (Kwon and Kim, 2010). To eliminate undesirable data and improve the quality of the data, this study applied the QC procedure to the observed CO_2 flux data.

The results of the estimated CO_2 and observed CO_2 are shown in Fig. 5(a). The coefficient of determination (R^2; Legates and McCabe 1999) values between the estimated CO_2 and the observed CO_2 from the flux tower for 3 years (2010–2012) were 0.50, 0.55, and 0.61. The CO_2 from MODIS GPP was also estimated with a Nash-Sutcliffe efficiency (NSE) of 0.35, 0.44, and 0.53. Donigian (2000) reported that R^2 values of less than 0.6, from 0.6 to 0.7, from 0.7 to 0.8, and greater than 0.8 are classified as poor, fair, good, and very good, respectively. Moriasi et al. (2007) recommended that performance ratings of NSE less than 0.5, from 0.5 to 0.65, from 0.65 to 0.75, and greater than 0.75 are classified as unsatisfactory, satisfactory, good, and very good, respectively. In the study watershed, the estimated CO_2 shows a maximum

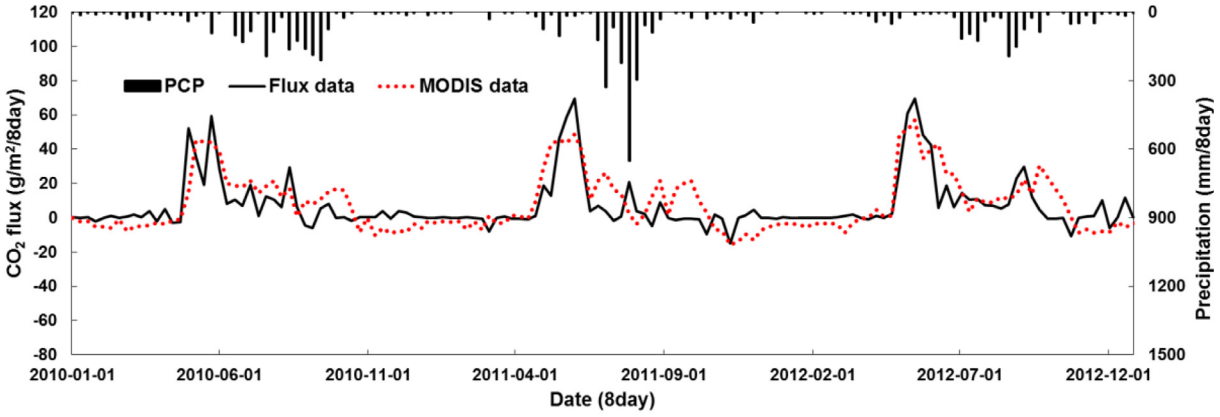

(a)

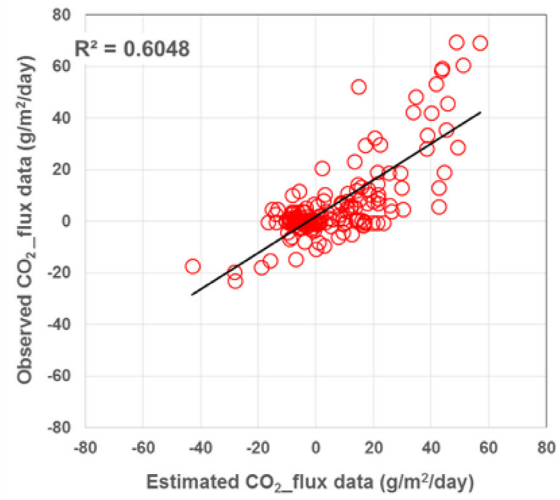

(b)

Fig. 5. CO_2 flux results: (a) CO_2 flux graph and (b) relationship between the observed CO_2 flux and the estimated CO_2 flux derived from MODIS GPP.

CO_2 load from May to June. Moreover, the results show that CO_2 decreased during the summer season, which represents a natural tendency of CO_2 declines during the rainy season in summer because of the monsoon climate in South Korea. In addition, the CO_2 flux generally recorded negative values during the rainy season in summer and maintained positive values for the other periods. This R^2 rating generally indicates good performance (Santhi et al., 2001; Van Liew et al., 2007).

These seasonal differences illustrate the influence of the principal soils and vegetation type at the sites between the flux tower and the MODIS pixel. The flux tower is located in a forested area, whereas the MODIS satellite data with a 500-m spatial resolution may include other land uses in addition to forests. Moreover, the difference between the two results indicates that the range of uncertainly was caused by the use of the eddy covariance method to measure the flux data. The sum of the sensible and latent heats measured using eddy covariance is commonly found to be lower than the available energy (Blanken et al., 1997; Goulden et al., 1996), which is the so-called energy closure problem. Finnigan et al. (2003) addressed this problem and concluded that a certain amount of flux may be lost when the averaging period is too small to capture low-frequency components of the covariance between the vertical velocity and the scalar of interest. These results indicate that the correlation between the observed CO_2 and estimated CO_2 from MODIS GPP was a good performance. Nevertheless, the reason for the low NSE less than 0.6 was that the satellite GPP was not matched completely with the observed GPP. It was difficult to improve the accuracy of the satellite GPP because it is not easy to measure the GPP.

To apply the SWAT model, the annual load of the estimated CO_2 flux is changed to the annual concentration (ppm) using the flux tower height (Table 1). The SWAT default CO_2 concentration is 330.0 ppm, whereas the estimated CO_2 concentration increased from 351.7 to 404.9 for 3 years. The deviation between the estimated CO_2 and the SWAT default CO_2 ranged from 51.7 ppm to 74.9 ppm. This result indicates that the CO_2 concentration consistently increased over the CO_2 measurement period at the three sites in South Korea (Table 1).

Table 1
Estimated CO_2 concentration (Korea Meteorological Administration, 2015).

Year	Estimated CO_2 concentration from MODIS GPP and Lloyd and Taylor method (ppm)	Measured CO_2 concentration (ppm)		
		Anmyeondo	Gosan	Ulleungdo
SWAT default	330.0			
2010	351.7	394.9	402.9	–
2011	375.2	396.8	404.2	403.1
2012	404.9	399.9	406.5	404.2

Table 2
Calibrated SWAT model parameters.

Parameter	Definition	Bound		Sensitivity	Adjusted Value
Streamflow (Q)					
CN2	SCS curve number for moisture condition	35	98	High	+5
Surlag	Surface runoff lag coefficient	1	24	Medium	24
GWQMN	Threshold bathymetry in the shallow aquifer required for return flow (mm)	0	100	High	0
GW_DELAY	Groundwater delay (days)	0	500	High	61
GW_REVAP	Groundwater evaporation coefficient	0.02	0.2	Medium	0.2
RCHRG_DP	Deep aquifer percolation coefficient	0	1	Medium	0.5
Evapotranspiration (ET)					
ESCO	Soil evaporation compensation coefficient	0	1	High	0.01
EPCO	Plant uptake compensation coefficient	0	1	High	1
CANMX	Maximum canopy storage (mm)	0	100	High	5
Soil moisture (SM)					
SOL_AWC	Available water capacity	0	1	High	0.14
SOL_K	Saturated hydraulic conductivity (mm/hr)	0	2000	High	25.8

3.4. Calibration and verification of the SWAT model

Prior to the model calibration and verification, a sensitivity analysis was conducted for the input parameters associated with streamflow, ET and SM. Table 2 represents the selected parameters regarding each of the hydrological components for the calibrated results. The R^2, Nash and Sutcliffe (1970) model efficiency (NSE), the root-mean-square error (RMSE), and the percent bias (PBIAS) were used to assess the accuracy of the SWAT model results via comparisons with the observed hydrological data. The NSE ranges from $-\infty$ to 1. A value of 1 corresponds to a perfect match between the simulated and observed data. A value of 0 indicates that the model predictions are as accurate as the mean of the observed data, whereas an efficiency of less than zero (NSE < 0) occurs when the observed mean is a better predictor. PBIAS is the deviation in the evaluated data, and it is expressed as a percentage (Moriasi et al., 2007).

The SWAT model was calibrated using the CO_2 concentration estimated from the streamflow data measured at the watershed outlet and the ET and SM data measured at the flux tower in the mixed forest area. The SWAT model was calibrated and verified using the six-year (2007–2012) streamflow data. The calibration period is the three-year period from 2007 to 2009, and the verification period is the three-year period from 2010 to 2012. The simulated ET and SM were simultaneously calibrated using data of 2009–2010 and verified using data of 2011–2012 measured at the flux tower. Table 3 shows the statistical streamflow results over 6 years. Table 4 summarizes the four-year calibration results for the ET and SM. Fig. 6 compares the observed and simulated streamflow, ET and SM. The average R^2 and NSE for the streamflow were 0.80 and 0.74, respectively. In addition, the average R^2 values for ET and SM were 0.77 and 0.80, respectively. The RMSE values for ET during the calibration and verification periods were 2.3 mm/day and 9.1 mm/day, respectively. In this study watershed, the PBIAS was between 9.6% and 30.2% for ET. These results indicate consensus between the observed ET and the simulated ET of more than 70%.

Table 3
Calibration and validation results for streamflow.

Year	PCP[#] (mm)	Runoff (mm)		Runoff ratio (%)		NSE[*]	$R^{2\dagger}$	Note
		Obs.	Sim.	Obs.	Sim.			
2007	1262.2	761.0	651.0	0.60	0.52	0.72	0.73	C[‡]
2008	1498.3	941.7	873.5	0.63	0.58	0.86	0.86	C[‡]
2009	1351.7	1000.9	808.3	0.74	0.60	0.87	0.83	C[‡]
2010	1853.5	1410.4	1221.6	0.76	0.66	0.72	0.78	V[§]
2011	1936.5	1563.9	1307.1	0.80	0.68	0.81	0.84	V[§]
2012	1455.3	772.2	909.9	0.53	0.63	0.45	0.73	V[§]
Mean	1559.6	1075.0	961.9	0.68	0.61	0.74	0.80	–

* NSE = Nash-Sutcliffe model efficiency.
† R^2 = coefficient of determination.
‡ C = calibration.
§ V = verification.
# PCP = Precipitation.

4. Impact on hydrologic components

Because this study area is small, it is difficult to observe changes in the hydrological components. To illustrate the changes, Table 5 shows the average monthly results for the hydrological components over 3 years (2010–2012), and it highlights the differences between the SWAT results that applied the estimated CO_2 and the default CO_2. The results of the ET based on the estimated CO_2 concentrations (351.7, 375.2, and 404.9 ppm) presented differences with the default SWAT values ranging from an average of −6.78 mm/month to an average of +0.42 mm/month over three years (ET based on the estimated CO_2 minus ET based on the default of 330 ppm). The results of the water yield (WY) based on the estimated CO_2 concentrations (351.7, 375.2, and 404.9 ppm) presented differences with the default SWAT values ranging from an average of −37.7 mm/month to an average of 33.3 mm/month for three years (WY based on the estimated CO_2 minus WY based on the default value of 330 ppm). The results of the soil water content (SW) based on the estimated CO_2 concentration (351.7, 375.2, and 404.9 ppm) presented differences with the default SWAT values ranging from an average of +1.5 mm/year to an average of +7.1 mm/year over three years (SW based on the estimated CO_2 minus the SW based on the default 330 ppm).

As shown in Table 5, throughout the study period (2010–2012), the ET based on the estimated CO_2 decreased by an average of 6.1%. The WY based on the estimated CO_2 increased by an average of 2.6% compared with the result using the default ET (330 ppm). The SW based on the estimated CO_2 increased by an average of 25.9%. The WY, ET, and SM are presented based on the depth unit per unit area (mm/km^2). If the SWAT model simulated the hydrologic components using the default CO_2 condition (330 ppm), then the WY, ET and SM would show inaccurate values.

Fig. 7 compares the monthly water balance between surface water and groundwater when applying the estimated CO_2 and the default CO_2. An analysis of the simulation results demonstrated that the temporal distribution of the SW and groundwater periods was strongly controlled from the surface runoff (SQ) and ET processes. This precipitation is consumed by the following components: ET (26.4% when applying the estimated CO_2 and 27.7% when applying the default CO_2), total runoff (TQ) at the basin outlet (67.3% when applying the estimated CO_2 and 64.9% when applying the default CO_2). In particular, the ratio of ET to precipitation for the default CO_2 was higher than that

Table 4
Calibration and validation results for evapotranspiration and soil moisture.

Period	R^2		NSE*		RMSE‡ (%/day)		PBIAS§ (%)	
	ET (mm)	SM (%)	ET (mm)	SM (%)	ET (mm)	SM (%)	ET	SM
Calibration period (2009–2010)	0.87	0.85	0.64	0.72	2.3	2.1	9.6	0.1
Validation period (2011–2012)	0.73	0.75	0.45	0.57	9.1	2.2	30.2	6.1

†R^2 = coefficient of determination.
* NSE = Nash-Sutcliffe model efficiency.
‡ RMSE = root-mean-square error.
§ PBIAS = percent bias.

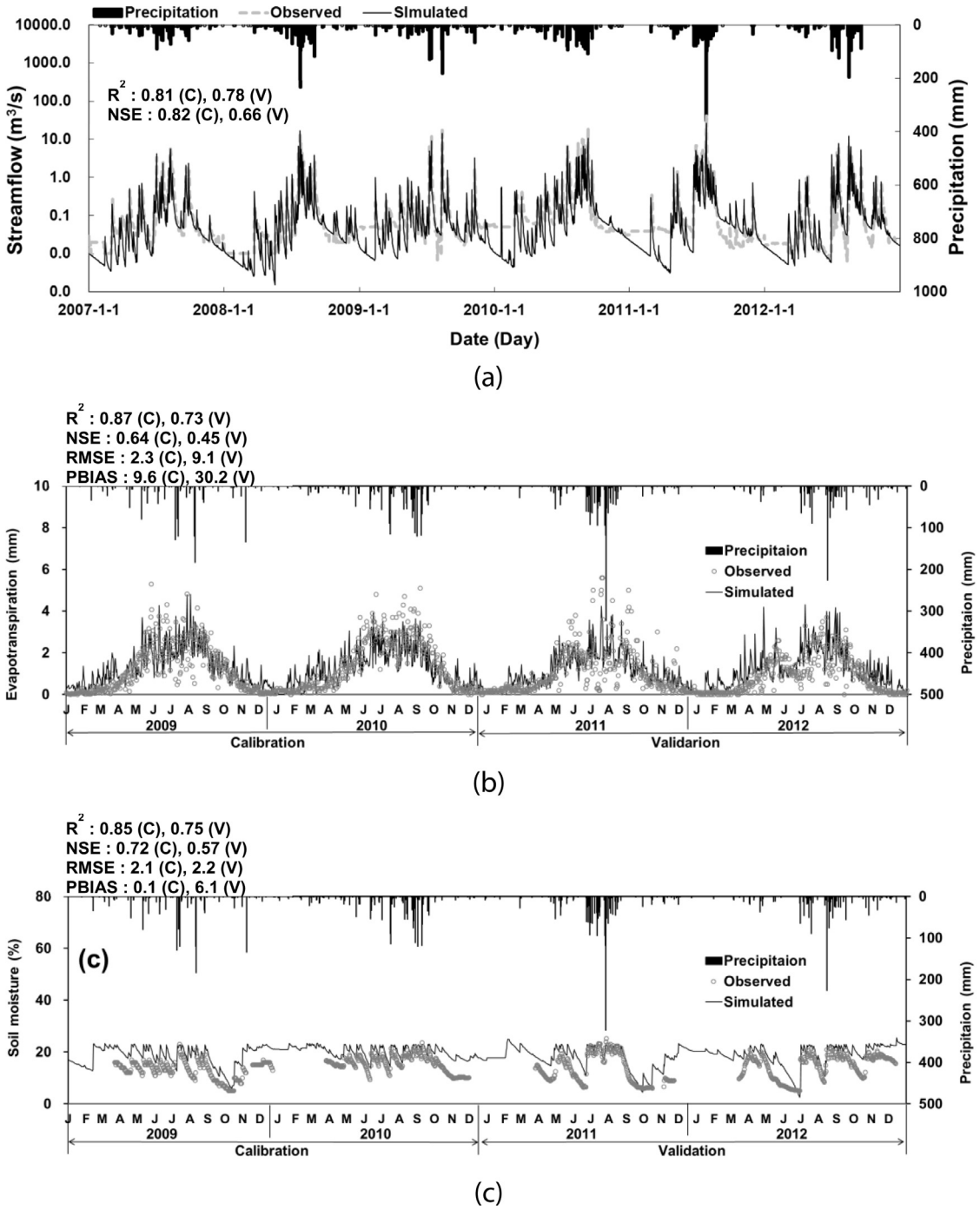

Fig. 6. Comparison of the measured and simulated (a) streamflow, (b) evapotranspiration (ET), and (c) soil moisture (SM).

Table 5
Summary of the average monthly hydrological components from 2010 to 2012.

Month	WY (mm)			ET (mm)			SW (mm)		
	Default CO_2	Estimated CO_2	Diff.*	Default CO_2	Estimated CO_2	Diff.*	Default CO_2	Estimated CO_2	Diff.*
1	10.3	12.6	2.3	5.87	5.76	−0.11	14.2	19.1	4.9
2	9.7	11.9	2.2	7.64	7.75	0.11	17.0	21.5	4.5
3	19.1	23.2	4.1	16.78	16.83	0.05	15.1	20.3	5.2
4	23.3	25.6	2.3	25.42	25.84	0.42	20.8	22.3	1.5
5	42.4	42.2	−0.3	44.85	40.62	−4.23	15.0	20.8	5.8
6	59.4	64.7	5.2	39.00	34.26	−4.74	17.6	22.7	5.1
7	301.2	334.6	33.3	71.31	64.53	−6.78	26.7	32.4	5.6
8	224.9	187.2	−37.7	67.92	65.00	−2.92	25.5	27.8	2.3
9	123.0	124.4	1.4	43.27	41.27	−2.00	21.0	26.6	5.6
10	34.6	38.2	3.6	25.86	24.28	−1.59	18.9	24.5	5.6
11	26.5	30.5	4.1	20.87	19.88	−0.99	22.5	29.2	6.7
12	16.4	19.0	2.6	12.07	11.85	−0.23	17.4	24.4	7.1
Total	890.9	914.1	23.2	380.87	357.86	−23.02	231.7	291.5	59.9

* Diff. = difference (SWAT result based on the estimated CO_2 minus SWAT result based on the default CO_2).

for the estimated CO_2, and these results controlled TQ, including the SQ and lateral runoff (LQ). When applying the estimated CO_2, the SQ increased and the LQ decreased. This phenomenon can be explained by plant transpiration. When transpiration decreased under the increasing the CO_2 concentration, the SW increased inversely. The increased SW caused the soil to become easily saturated, and the saturated soils increased the SQ and reduced the LQ.

These results indicate that the hydrologic components significantly

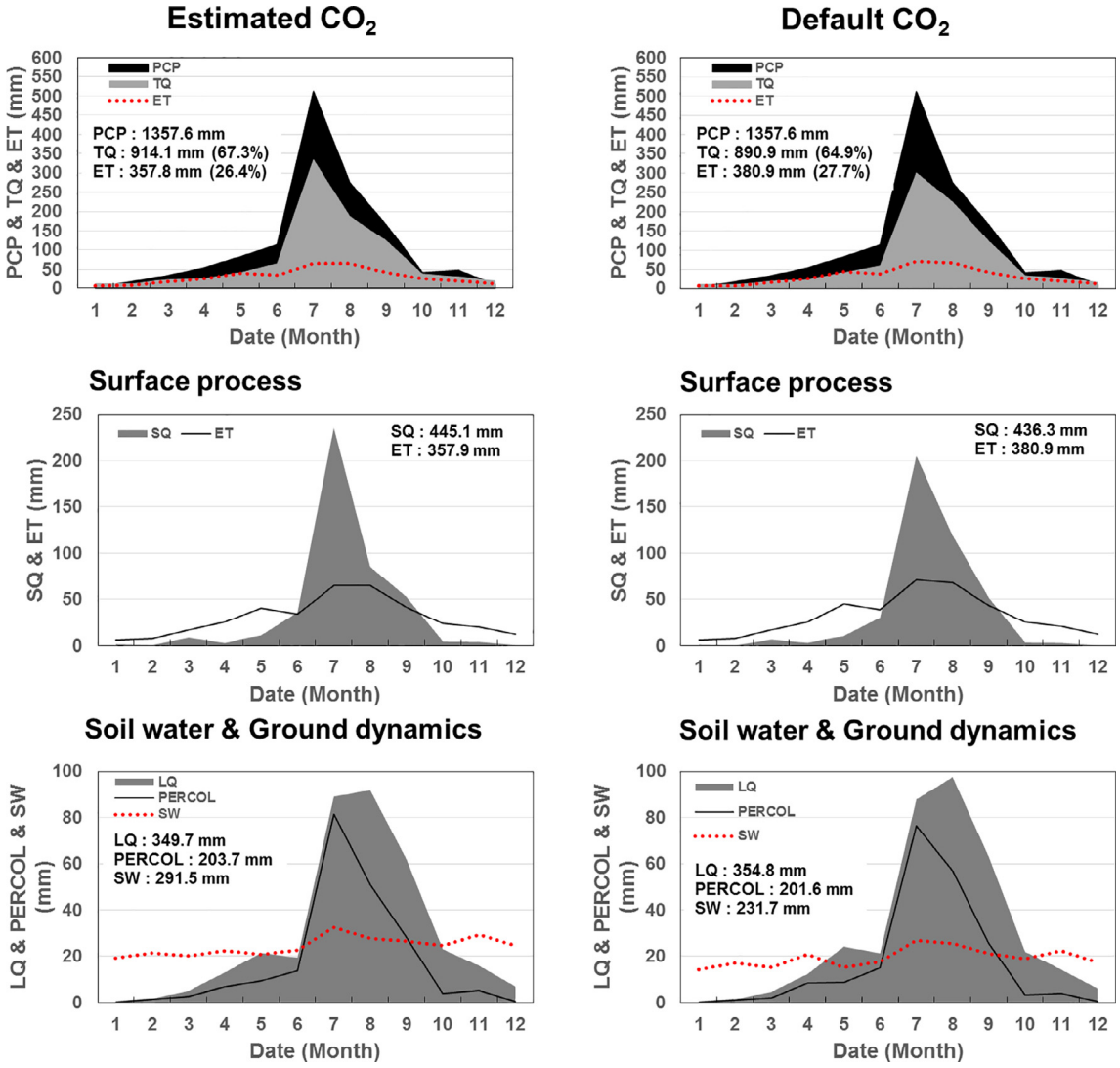

Fig. 7. Comparison of the monthly water balance components considering interactions between the surface water and the groundwater when applying the estimated CO_2 and the default CO_2: total runoff (TQ), surface runoff (SQ), lateral runoff (LQ), evapotranspiration (ET), percolation (PERCOL), and soil water content (SW).

changed in this watershed. CO_2 causes a physiological reaction on plant stomata. The appropriateness of these results can be proved by comparing the existing experimental study. Chun et al. (2011) investigated water uptake and quantified water-use efficiency under ambient and elevated CO_2 combined with four water-stress levels in experimental plots. In both well-watered and water-stressed conditions, approximately 13–20% and 35% less water was used under elevated CO_2 conditions (800 μmol mol^{-1}) than under ambient CO_2 conditions (400 μmol mol^{-1}) for water-stressed conditions and well-watered conditions, respectively. These results suggest that under increased CO_2 concentrations, as generally predicted in the future, less water will be required for plants than at present up to the limit.

This can be attributed to reduced transpiration in vegetation. Increases in atmospheric CO_2 increase the leaf's internal CO_2 absorption rate, and the plants react by increasing the stomatal resistance, which reduces transpiration from the leaf into the atmosphere (Morison and Gifford, 1984). This reaction reduces the plant's water-use requirements and increases the plant's water-use efficiency. Under increased CO_2 concentrations, stomatal responses regulate photosynthesis (Ramirez Jorge and Finnerty, 1996).

4.1. Water cycle condition obtained using the Budyko curve

To quantify the relative contributions of climate and direct human impacts to streamflow, a hydrologic model is required to link both climatic forcing and human impacts with the hydrological response. In this study, climatic and anthropogenic impacts induced changes in the CO_2 concentration over the 6-year period from 2007 to 2012. This study is focused on changes in the atmospheric CO_2 concentration. The watersheds have changed due to the CO_2 change. Thus, watersheds are not on the same Budyko-type curve. The differences in Budyko-type curves depend on the physical properties of the watersheds.

The water-energy balance at the watershed scale over a long-term temporal scale describes the partitioning of precipitation (P) into evaporation and runoff. Budyko (1958) postulated that the mean annual evaporation from a watershed could be determined to first order from rainfall and net radiation. The ratio of the mean annual evaporation (E) to the mean annual precipitation (E/P, evaporation ratio) is primarily controlled by the ratio of the mean annual potential evaporation (PET) to the mean annual precipitation (PET/P, climatic dryness index) as shown in Fig. 8.

Based on this theory, vertical movement of the watershed from the Budyko-type curve can be divided into climate-induced and direct human-induced changes. Four possible movement directions are observed for a watershed. If the watershed moves to the top right corner, then the climate and direct human interferences affect the streamflow (R) in the same direction by decreasing the runoff coefficient (R = Q/P), whereas if the watershed moves to the bottom left corner, then climate and humans caused the increased and decreased runoff coefficients, respectively (Wang and Hejazi, 2011).

Fig. 8 shows that streamflow (R) increased and that the dryness index (including ET) decreased. The impacts of CO_2 change can induce both horizontal and vertical components, and both components can affect streamflow, whereas direct human interference can only induce a vertical component. As seen from Fig. 8, assuming that the Budyko graph based on the default CO_2 is the natural condition, the Budyko graph based on the estimated CO_2 moves forward as a whole. Thus, the results revealed that CO_2 changes driven by climate and human activity cause a change in the water cycle in the natural condition. Also, moving forward against the natural condition means that the dryness index decreases. Therefore, this means that the portion of evapotranspiration in the water cycle of the watershed became smaller, whereas the portion of runoff became larger. Finally, the changes in the Budyko graph show that the water cycle condition in this study moved the wet condition by the CO_2 concentration.

5. Summary and conclusions

This study attempted to assess the impact of potential CO_2 changes on the hydrologic components in the forest-dominant Seolma-cheon watershed (8.48 km^2) of South Korea by using the Terra MODIS GPP, the Lloyd and Taylor method, and the SWAT model. The model was calibrated and verified based on the streamflow, ET and SM values obtained from the estimated CO_2 concentration. The average R^2 values for the ET and SM were 0.77 and 0.80, respectively. To estimate the CO_2 flux derived from the MODIS GPP, the MODIS GPP product, which is an 8-day composite at a 1-km spatial resolution, was adopted to determine the spatial CO_2 flux. The MODIS GPP data were corrected using the QC flag. The MODIS CO_2 flux was estimated as the sum of GPP and R_{ec} using the Lloyd and Taylor method (1994). The CO_2 concentrations were estimated based on satellite images and observed CO_2 concentrations, and the R^2 between the estimated CO_2 from MODIS GPP and the observed CO_2 from the flux tower for 3 years (2010–2012) was 0.61. This R^2 value generally denotes good performance. To apply

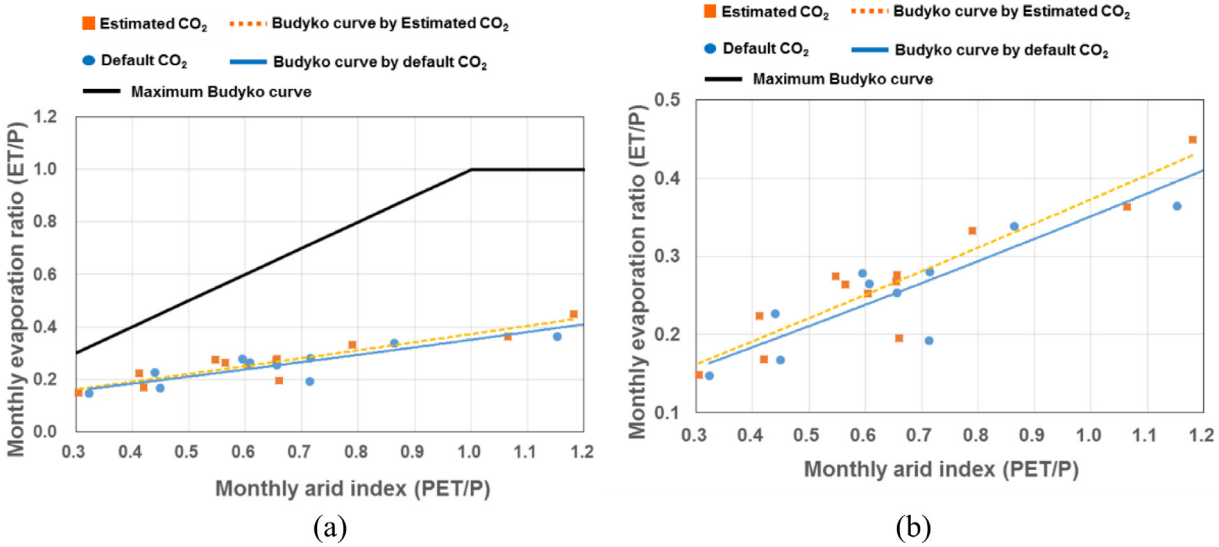

Fig. 8. Distribution of the mean annual evaporation ratio (E/P) versus the mean annual arid index (PET/P) based on the data over two sub-periods in 33 catchments. The Budyko curves calculated by Eq. (4) are plotted as solid lines: (a) the total range and (b) a specific range of the Budyko curves.

for the SWAT model, the annual CO_2 flux load derived from the satellite image was rescaled to the annual concentration in ppm using data collected at each height of the flux tower. The SWAT default CO_2 concentration is 330.0 ppm, whereas the estimated CO_2 concentration derived from MODIS GPP increased from 351.7 to 404.9 ppm over 3 years. The deviation between the satellite CO_2 concentration and the SWAT default CO_2 concentration ranged from 51.7 ppm to 74.9 ppm. This result shows that the CO_2 concentration increased in South Korea during the study period.

To analyse the changes in the water cycle, we evaluated hydrologic components such as the TQ, SQ, LQ, SW, and ET and then derived Budyko curves. The curves indicate that the impact of CO_2 change can induce both horizontal and vertical components which affect streamflow, whereas direct human interference has decreasing influence on a vertical component only. The results showed that the streamflow increased and the dryness index (including ET) decreased. As a result, the conservation of soil moisture and reduction of transpiration attributable to increased CO_2 concentration could have a significant impact on the overall water cycle in the watershed.

Beyond simple runoff modelling, hydrologic modelling should be applied to determine the interactions between atmosphere and land. Notably, accurate assessments of ET are essential to evaluate the potential range of responses in the water cycle. This study revealed that the estimated CO_2 concentration affects the direction, magnitude, and spatial distribution of hydrological responses. These findings will provide useful insights for advancing watershed management technology and policies. Usually, data on hydrological components collected over a period greater than five years are required to analyse the water cycle using Budyko curves. Thus, future research studies should obtain hydrological data for periods greater than five years and perform predictions based on a greater amount of observed data to improve upon the results presented here.

Acknowledgements

This research was supported by a grant (18AWMP-B079625-05) from Water Management Research Program sponsored by the Ministry of Land, Infrastructure and Transport of the Korean government.

References

Korea Meteorological Administration, 2015. In: Report on Global Atmosphere Watch. Korea Meteorological Administration, South Korea, pp. 5–16 (in Korean).
Ahn, S.R., Heong, J.H., Kim, S.J., 2016. Assessing drought threats to agricultural water supplies under climate change by combining the SWAT and MODSIM models for the Geum River basin, South Korea. Hydrol. Sci. J 10.1080/02626667.2015.1112905.
Alexandridis, T.K., Cherif, I., Kalogeropoulos, C., Monachou, S., Eskridge, K., Silleos, N., 2013. Rapid error assessment for quantitative estimations from Landsat 7 gap = filled images. Remote Sens. Lett. 4 (9), 920–928.
Arnold, J.G., Srinivasan, R., Muttiah, R.S., Williams, J.R., 2008. Large area hydrologic modeling and assessment part i: model development. J. Am. Water Resour. Assoc. 34 (1), 73–89.
Blanken, P.D., Black, T.A., Yang, P.C., Neumann, H.H., Nesic, Z., Staebler, R., den Hartog, G., Novak, M.D., Lee, X., 1997. Energy balance and canopy conductance of a boreal aspen forest: partitioning overstory and understory components. J. Geophys. Res. 102 (24), 28915–28927.
Budyko, M.I., 1974. In: Climate and Life. Academic, New York, pp. 508.
Choudhury, B.J., 1999. Evaluation of an equation for annual evaporation using field observations and results from a biophysical model. J. Hydrol. 216, 99–110.
Chun, J.A., Wang, Q., Timlin, D., Fleisher, D., Reddy, V.R., 2011. Effect of elevated carbon dioxide and water stress on gas exchange and water use efficiency in corn. Agric. For. Meteorol. 151, 378–384.
Donigian, Jr., A.S. 2000. HSPF Training Workshop Handbook and CD. Lecture #19, Calibraion and Verification Issures, Slide #L19-22 EPA Headquarters, Presented and prepared for US EPA.
Donohue, R.J., Roderick, M.L., McVicar, T.R., 2007. On the importance of including vegetation dynamics in Budyko's hydrological model. Hydrol. Earth Syst. Sci. 11, 983–995.
Donohue, R.J., Roderick, M.L., McVicar, T.R., 2010. Can dynamic vegetation information improve the accuracy of Budyko's hydrological model. J. Hydrol. 390, 23–34.
Finnigan, J.J., Clement, R., Malhi, Y., Leuning, R., Cleugh, H.A., 2003. A re-evaluation of long-term flux measurement techniques, part I: Averaging and coordinate rotation. Boundary-Layer Meteorol. 107, 1–48.
Gerrits, A.M., Savenije, H.H.G., Veling, E.J.M., Pfister, L., 2009. Analytical derivation of the Budyko curve based on rainfall characteristics and a simple evaporation model. Water Resour. Res. 45, W04403. http://dx.doi.org/10.1029/2008WR007308.
Goulden, M.L., Munger, J.W., Fan, S.M., Daube, B.C., Wofsy, S.C., 1996. Measurements of carbon sequestration by long-term eddy covariance: method and a critical evaluation of accuracy. Global Change Biol. 2, 169–182.
Heinsch, F.A., Reeves, M., Votava, P., Kang, S., Milesi, C., Zhao, M., Glassy, J., Jolly, W.M., Kimball, J.S., Nemannpi, R.R., Running, S.W., 2003. User's guide GPP and NPP (MOD17A2/A3) products NASA MODIS land algorithm, numerical terradynamic simulation group. In: MOD17 User's Guide. University of Montana, USA, pp. 1–57.
Hong, J., Kwon, H., Lim, J.H., Byun, Y.H., Lee, J., Kim, J., 2009. Standardization of KoFlux eddy-covariance data processing. Korean J. Agric. For. Meteorol. 11 (1), 19–26 (in Korean).
Jothityangkoon, C., Sivapalan, M., 2009. Framework for exploration of climatic and landscape controls on catchment water balance, with emphasis on inter-annual variability. J. Hydrol. 371, 154–168.
Jung, C.G., Lee, D.R., Moon, J.W., 2014. Comparison of the Penman Monteith and regional calibration of Hargreaves equation for actual evapotranspiration using SWAT stimulated results in Seolma-Cheon watershed. Hydrol. Sci J 10.1080/02626667.2014.943231.
Justice, C.O., Vermote, E., Townshend, J.R.G., Defries, R., Roy, D.P., Hall, D.K., Salomonson, V.V., Privette, J.L., Riggs, G., Strahler, A., Lucht, W., Myneni, R.B., Knyazikhin, Y., Running, S.W., Nemani, R.R., Wan, Z., Huete, A.R., van Leeuwen, W., Wolfe, R.E., Giglio, L., Muller, J., Lewis, P., Barnsley, M.J., 1998. The moderate resolution imaging spectroradiometer (MODIS): land remote sensing for global change research. IEEE Trans. Geosci. Remote Sens. 36, 1228–1249.
Justice, C.O., Townshend, J.R.G., Vermote, E.F., Masuoka, E., Wolfe, R.E., Saleous, N., Roy, D.P., Morisette, J.T., 2002. An overview of MODIS land data processing and product status. Remote Sens. Environ. 83, 3–15. http://dx.doi.org/10.1016/S0034-4257(02)00084-6.
Kimball, B.A., Idso, S.B., 1983. Increasing atmospheric CO_2: effects on crop yield, water use and climate. Agric. Water Manage. 7, 55–72.
Kwon, H., Kim, J., 2010. KoFlux issue: KoFlux's progress: background, status and direction. Korean J. Agric. For. Meteorol. 12 (4), 241–263 (in Korean).
Legates, D.R., McCabe, G.J., 1999. Evaluating the use of goodness-of-fit measures in hydrologic and model validation. Water Resour. Res. 35, 233–241.
Lloyd, J., Taylor, J.A., 1994. On the temperature dependence of soil respiration. Funct. Ecol. 8, 315–323.
Milly, P.C.D., 1994. Climate, soil water storage, and the average annual water balance. Water Resour. Res. 30 (7), 2143–2156. http://dx.doi.org/10.1029/94WR00586.
Monteith, J.L., Moss, C.J., 1977. Climate and the efficiency of crop production in Britain [and discussion]. Philos. Trans. R. Soc. London B Biol. Sci. 281, 277–294.
Monteith, J.L., 1972. Solar radiation and productivity in tropical ecosystems. J. Appl. Ecol. 747–766.
Moriasi, D.N., Arnold, J.G., Van Liew, M.W., Bingner, R.L., Harmel, R.D., Veith, T.L., 2007. Model evaluation guidelines for systematic quantification of accuracy in watershed simulations. Am. Soc. Agric. Biol. Eng. 50, 885–900. http://dx.doi.org/10.13031/2013.23153.
Morison, J.I.L., 1987. Intercellular CO_2 concentration and stomatal response to CO_2. Plant growth and water use with limited water sully in high CO_2 concentrations. In: Zeiger, E., Cowan, I.R., Farquhar, G.D. (Eds.), Stomatal Function. Stanford University Press, Stanford, CA, USA, pp. 229–251.
Morison, J.I.L., Gifford, R.M., 1984. Plant growth and water use with limited water sully in high CO_2 concentrations. leaf area, water use and transpiration. Aust. J. Plant Physiol. 11, 361–374.
Nash, J.E., Sutcliffe, J.V., 1970. River flow forecasting through conceptual models: part I. a discussion of principles. J. Hydrol. 10 (3), 283–290.
Neitsch, S.L., Arnold, J.G., Kiniry, J.R., Srinivasan, R., Williams, J.R., 2005. Soil and water assessment tool input/output file documentation version 2004: Draft-September 2005. Blackland: Grassland, Soil and Water Research Laboratory, Agricultural Research Service, Temple, Texais USA.
Neitsch, S.L., Arnold, J.G., Kiniry, J.R., Williams, J.R., 2001. Soil and Water Assessment Tool: Theoretical Documentation, Version 2000. Draft (April 2001). USDA-ARS Grassland, Soil and Water Research Laboratory and Blackland Research Center, Temple, Tex.
Nemani, R.R., Keeling, C.D., Hashimoto, H., Jolly, W.M., Piper, S.C., Tucker, C.J., Myneni, R.B., Running, S.W., 2003. Climate-driven increases in global terrestrial net primary production from 1982 to 1999. Science 300, 1560–1562.
Ni, H., Jin, S.H., Zheng, N., 2013. Estimating the spatial pattern of soil respiration in Tibetan alpine grasslands using Landsat TM images and MODIS data. Ecol. Indic. 26, 117–125.
Pike, J.G., 1964. The estimation of annual runoff from meteorological data in a tropical climate. J. Hydrol. 2116–2123.
Ramirez Jorge, A., Finnerty, B., 1996. CO_2 and temperature effects on evapotranspiration and irrigated agriculture. J. Irrig. Drain. Eng. 122 (3), 155–163.
Reichstein, M., Falge, E., Baldocchi, D., Papale, D., Aubinet, M., Berbigier, P., Bernhofer, C., Buchmann, N., Gilmanov, T., Granier, A., Grunwald, T., Havrankova, K., Ilvesniemi, H., Janous, D., Knohl, A., Laurila, T., Lohila, A., Loustau, D., Matteucci, G., Meyers, T., Miglietta, F., Ourcival, J.M., Pumpanen, J., Rambal, S., Rotenberg, E., Sanz, M., Tenhunen, J., Seufert, G., Vaccari, F., Vesala, T., Yakir, D., Valentini, R., 2005. On the separation of net ecosystem exchange into assimilation and ecosystem respiration: review and improved algorithm. Global Change Biol. 11 (9), 1424–1439.
Roderick, M.L., Farquhar, G.D., 2011. A simple framework for relating variations in runoff to variations in climatic conditions and catchment properties. Water Resour. Res. 47http://dx.doi.org/10.1029/2010WR009826. W00G07.
Saigusa, N., Yamamoto, S., Murayama, S., Kondo, H., Nishimura, N., 2002. Gross primary

production and net ecosystem exchange of a cool-temperate deciduous forest estimated by the eddy covariance method. Agric. For. Meteorol. 112, 203–215.
Santhi, C.J., Arnold, G., Williams, J.R., Dugas, W.A., Srinivasan, R., Hauck, L.M., 2001. Validation of the SWAT model on a large river basin with point and nonpoint sources. J. Am. Water Resour. Assoc. 37 (5), 1169–1188.
Sims, D.A., Rahman, A.F., Cordova, V.D., El-Masri, B.Z., Baldocchi, D.D., Flanagan, L.B., Goldstein, A.H., Hollinger, D.Y., Mission, L., Monson, R.K., Oechel, W.C., Schmid, H.P., Wofsy, S.C., Xu, L., 2006. On the use of MODIS EVI to assess gross primary productivity of North American ecosystems. J. Geophys. Res. 111http://dx.doi.org/10.1029/2006JG000162. G04015.
Thornton, P.E., Law, B.E., Gholz, H.L., Clark, K.L., Falge, E., Ellsworth, D.S., Goldstein, A.H., Monson, R.K., Hollinger, D., Falk, M., Chen, J., Sparks, P., 2002. Modeling and measuring the effects of disturbance history and climate on carbon and water budgets in evergreen needle leaf forests. Agric. For. Meteorol. 113, 185–222.
Turner, D.P., Ritts, W.D., Cohen, W.B., Gower, S.T., Zhao, M.S., Running, S.W., Wofsy, S.C., Urbanski, S., Dunn, A.L., Munger, J.W., 2003. Scaling gross primary production (GPP) over boreal and deciduous forest landscapes in support of MODIS GPP product validation. Remote Sens. Environ. 88, 256–270.
Van Gorsel, E., Leuning, R., Cleugh, H., Keith, H., Suni, T., 2007. Nocturnal carbon efflux: reconciliation of eddy covariance and chamber measurements using an alternative to the u*-threshold filtering. Tellus 59B, 397–403.
Van Liew, M.W., Veith, T.L., Bosch, D.D., Arnold, J.G., 2007. Suitability of SWAT for the conservation effects assessment project: A comparison on USDA-ARS experimental watersheds. J. Hydrol. Eng. 12 (2), 173–189.
Wang, D., Hejazi, M., 2011. Quantifying the relative contribution of the climate and direct human impacts on mean annual streamflow in the contiguous United States. Water Resour. Res. 47http://dx.doi.org/10.1029/2010WR010283. W00J12.
Wang, Z., Xiao, X., Yan, X., 2010. Modeling gross primary production of maize cropland and degraded grassland in northeastern China. Agric. For. Meteorol. 150, 1160–1167.
Wen, K.F., Yu, G.R., Sun, X.M., Li, Q.K., Liu, Y.F., Zhang, L.M., Ren, C.Y., Fu, Y.L., Li, Z.Q., 2006. Soil moisture effect on the temperature dependence of ecosystem respiration in a subtropical Pinus plantation of southeastern China. Agric. For. Meteorol. 137, 166–175.
Wu, Y., Liu, S., Abdul-Aziz, O.I., 2012. Hydrological effects of the increased CO_2 and climate change in the Upper Mississippi River Basin using a modified SWAT. Clim. Change 110, 977–1003.
Yang, D., Shao, W., Yeh, P.J.F., Yang, H., Kanae, S., Oki, T., 2009. Impact of vegetation coverage on regional water balance in the nonhumid regions of China. Water Resour. Res. 45 W00A14.
Yang, D., Sun, F., Liu, Z., Cong, Z., Ni, G., Lei, Z., 2007. Analyzing spatial and temporal variability of annual water-energy balance in nonhumid regions of China using the Budyko hypothesis. Water Resour. Res. 43 (4). http://dx.doi.org/10.1029/2006WR005224.
Yang, H., Yang, D., Lei, Z., Sun, F., 2008. New analytical derivation of the mean annual water-energy balance equation. Water Resour. Res. 44, W034103.
Zhang, L.W., Dawes, R., Walker, G.R., 2001. Response of mean annual evapotranspiration to vegetation changes at catchment scale. Water Resour. Res. 37 (3), 701–708. http://dx.doi.org/10.1029/2000WR900325.
Zhao, M., Running, S.W., Heinsch, F.A., Nemani, R.R., 2011. In: MODIS derived terrestrial primary production. In: Land Remote Sensing and Global Environmental Change. Springer, New York, USA, pp. 635–660. http://dx.doi.org/10.1007/978-1-4419-6749-7_28.
Zhao, M., Running, S.W., 2010. Drought-induced reduction in global terrestrial net primary production from 2000 through 2009. Science 329, 940–943.